2-9-2017

A Low Assembly Cost Coaxial Magnetic Gearbox

Kiran Uppalapati
University of North Carolina at Charlotte

Joshua Kadel
University of North Carolina at Charlotte

Jason Wright
University of North Carolina at Charlotte

Kang Li
University of North Carolina at Charlotte

Wesley Williams
University of North Carolina at Charlotte

See next page for additional authors

A Low Assembly Cost Coaxial Magnetic Gearbox

K. Uppalapati†, J. Kadel*, J. Wright†, K. Li†, W. Williams*
*Department of Engineering Technology
†Department of Electrical and Computer Engineering
University of North Carolina at Charlotte
Charlotte, NC, USA
wbwillia@uncc.edu

J. Z. Bird
Laboratory for Electromechanical Energy Conversion and Control
Department of Electrical and Computer Engineering Portland State University
Portland, OR, USA
jonathan.bird@ieee.org

***Abstract*—This paper presents the design investigation and experimental testing of a flux-focusing magnetic gearbox with a three piece laminated rotor structure. Each rotor is made of a single lamination stack held together via thin lamination bridges. It is calculated that mechanical bridges reduces the torque density from 156Nm/L to 139Nm/L (a reduction of 11%). The experimentally measured torque density is shown to be only 95Nm/L because the magnets were demagnetized during testing.**

Keywords—flux focusing, gearbox, finite element analysis, permanent magnets

I. Introduction

Magnetic gearboxes (MG) utilize magnetic field heterodyning to create speed amplification without physical contact. MGs have an inherent torque overload capability and they have the potential for quiet operation and high conversion efficiency [1, 2]. The lack of physical contact between rotors will increase a MGs reliability and lower its maintenance cost since gear lubrication will not be required. An example of a coaxial flux-focusing MG is shown in Fig. 1. If the inner rotor contains p_1 pole-pairs and rotates at ω_1 and the outer rotor contains p_3 pole-pairs and rotates at ω_3 then if a middle cage rotor containing, n_2, steel segments is placed between the inner and outer rotors and the number of steel segments is [1, 2]

$$n_2 = p_1 + p_3 \tag{1}$$

then it can be shown that the angular speed relationship between each rotor is [1, 2]

$$n_2\omega_2 = p_1\omega_1 + p_3\omega_3 \tag{2}$$

where the subscripts denote rotor number. If the outer rotor is fixed ($\omega_3 = 0$) the speed ratio is

$$\omega_1 = G_{12}\omega_2 \tag{3}$$

where $G_{12} = n_2 / p_1$. For the example shown in Fig. 1 the gear ratio is G_{12}=4.25.

The power relation between rotors is

$$T_1\omega_1 - T_2\omega_2 = P_l \tag{4}$$

with P_l defined as

$$P_l = P_f + P_e \tag{5}$$

where P_f =friction and windage loss and P_e = eddy current and hysteresis loss. The torque on the central segmented cage rotor in (4) is shown as a negative as the torque on the cage rotor opposes the torque created on both the outer an inner rotor.

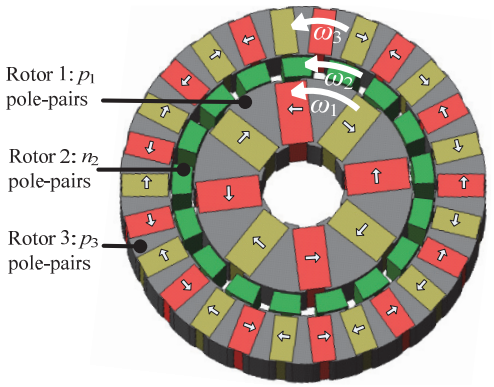

Fig. 1. A 4:25:1 coaxial flux-focusing magnetic gearbox using flux focusing PMs. p_1=4 pole-pairs, n_2=17 steel poles and p_3=13 pole-pairs on the outer rotor [3].

The active region volumetric torque density of a rotary machine can be compared by using

$$T_{vi} = T_2 / (\pi r_{o3}^2 d) \tag{6}$$

where T_2 = peak torque on rotor 2, r_{o3} = outer radius of MG and d = stack length. Coaxial MGs have been experimentally shown to be capable of achieving active region torque densities above 200 Nm/L [4]. However, further improvements in torque density are still needed in order to make them competitive with mechanical gearboxes. The mechanical assembly of the MG is perhaps one of the most challenging aspects of designing a MG and the central inner steel segments, called the cage rotor in this paper, are particularly difficult to design as they carry high torque and experience large oscillatory radial and azimuthal forces [5].

Atallah *et al.* constructed a MG in which the central segmented cage rotor was made of one laminated stack with outer radius bridges [2] the laminations were supported in place by using epoxy and non-magnetic stainless steels rods within the spaces below the steel bridges. Around the same time Rasmussen *et al.* independently designed a MG [6] using a flux focusing inner rotor and surface mounted outer magnets. The central steel segmented rotor was retained in place using nylon and stainless steel rods. In [7, 8] Rasmussen *et al.* and Gerber *et al.* tried using bridges on the inside diameter of the cage rotor with steel rods embedded in resin within the cage rotor

spacing. In a later design Rasmussen used a composite bar to secure the cage rotor in place [9]. This lowered the losses during high speed operation. Frank *et al.* constructed a MG using bridges on both the inner and outer cage rotor radii [10]. However, using bridges on both sides of the cage rotor will significantly lower the peak torque.

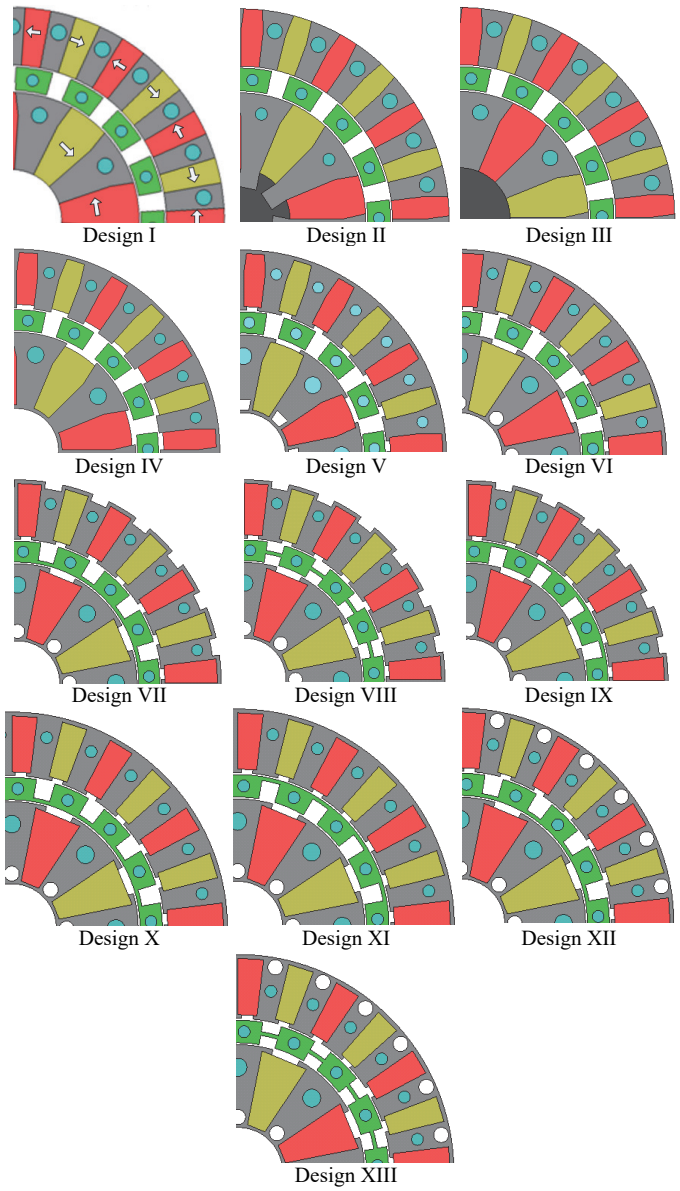

Fig. 2. Design topologies that were studied

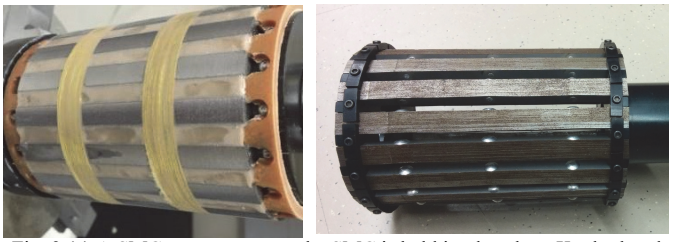

Fig. 3.(a) A SMC rotor structure, the SMC is held in place by a Kevlar band. and (b) a laminated cage rotor with laminations stacked along the azimuthal direction.

TABLE I
GEOMETRIC PARAMETERS AND MATERIAL PROPERTIES

Description		Value	Units
Inner rotor	Pole pairs, p_1	4	-
	Inner radius, r_{i1}	12	mm
	Outer radius, r_{o1}	33	mm
	Steel pole span, θ_{s1}	$\pi/8$	rad.
	Airgap, g	0.5	mm
Cage rotor	Steel poles, n_2	17	-
	Inner radius, r_{i1}	33.5	mm
	Outer radius, r_{o1}	39.5	mm
	Steel pole span, θ_{s2}	$7\pi/90$	rad.
Outer rotor (stationary)	Pole pairs, p_3	13	-
	Inner radius, r_{i3}	40	mm
	Outer radius, r_{o3}	56	mm
	Steel pole span, θ_{s3}	$\pi/26$	rad.
	Airgap, g	0.5	mm
Material	Magnet, NdFeB, N40H, B_r	1.25	T
	Laminations, M19 C5 G26	-	-
Active region stack length, d		75	mm

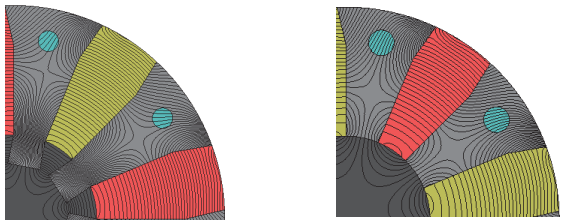

Fig. 4. Magnetic vector potential field lines for the inner rotor for (a) Design II and (b) Design III. The increased inner shaft field leakage in Design II is clearly evident

Rasmussen *et al.* [7], Gouda [11] and the authors of this paper tried constructing a MG cage rotor using soft magnetic composite (SMC) magnetic material. The authors SMC rotor is shown in Fig. 3(a). The SMC material is incredibly brittle and therefore retaining it in place is difficult for a MG application. Uppalapati *et al.* constructed a MG using solid steel bar segments [4]. Uppalapati showed that solid steel bars could only be used when operating with a very low input speed. In [12] Jian *et al.* successfully tested a MG in which it appears that the cage rotor laminations were supported only along one axial side of the rotor [12]. The authors of this paper also constructed a cage rotor using laminations stacked along the azimuthal length, as shown in Fig. 3(b) however, for such a design, it is difficult to secure the laminations in place.

Designs that require the cage rotor to be made with resin casting or are made from many individual steel pieces will increase construction cost significantly and also create tolerance and alignment challenges. This paper looks at the different design trade-offs when modifying a flux focusing MG with the emphasis on trying to design a low assembly cost MG structure whilst still retaining a relatively high torque density. The research builds on the work presented in [3].

II. DESIGN ANALYSIS

Using the parameters shown in Table I a MG volumetric torque density for the design shown in Fig. 1 was calculated to be $T_2 = 156$ Nm/L. However, this design is not practical from an assembly perspective because the steel poles are made of

individual steel segments [3]. In order to develop a lower assembly cost design a range of different design changes were considered, as shown in Fig. 2. A summary of the corresponding torque and the torque ripple for relevant designs is shown in Table II. The torque ripple value is computed at the peak torque condition.

Design I, II and III look at different steel pole configurations that will retain the magnets in place without the need for the tooth tips as used by the design shown in Fig. 1. The azimuthally directed flux-focusing magnetization direction is shown for Design I. All other designs shown in Fig. 2 use the same magnetization directions as that shown for Design I. The blue circles shown in Fig. 2 are used to retain the steel teeth in place via axially placed end plates. Design I and III have higher torque than the original design however Design II has lower torque due to the leakage that is created through the inner rotor retaining bars, this leakage is illustrated in Fig. 4.

Designs IV, V and VI look at the effect of adding steel bridges on the inner radii of the inner rotor and the outer radii of the outer rotor. Comparing Design III and IV one can note that the bridges reduce the torque by 5%. In Design V and VI flux leakage barriers (holes) have been inserted around the base of the inner rotor in addition magnet retaining lips have been added. The flux leakage barriers increase torque slightly while the magnet retaining lips reduce the torque. The overall changes therefore make minimal difference when compared to Design IV.

Design VII, VIII and IX look at the effect of adding steel bridges on the cage rotor. In addition, rectangular leakage barriers were added on the outer radius of the outer rotor. It can been seen from Table II that adding the bridges on the inner radius or center reduces the torque by ~7% when compared to Design VI while adding the bridge on the outer radius reduces peak torque by 14% compared to Design VI. Locating the rotor 2 bridges near the inner radius or center of the cage rotor results in a relatively large torque ripple being created whereas putting the rotor 2 bridges at the outer radii (Design IX) results in a low torque ripple but this also significantly reduces the peak torque. Based on these three designs it appears that there is a trade-off between achieving a low torque ripple or high peak torque. If one now considers Design X and XI in which the rectangular outer rotor leakage slots have been removed one can see that removing this outer rectangular slot does not change the torque ripple significantly (when compared to Design VII and IX). However, if the outer rotor rectangular leakage slot in Design VII is replaced with a circular hole as in Design XII it can be noted that the torque ripple drops significantly and torque increases slightly. Therefore, in this design the circular hole helps to reduce torque ripple.

Design XIII shifts the cage rotor bridge to the center and one can see that the torque ripple goes down considerably but the peak torque only reduces by 2.8Nm therefore Design XIII was selected. The final design (Design XIV) is shown in Fig. 5. Design XIV differs slightly from Design XIII in that additional outer and inner slots were added for mechanical outer sleeve retention purposes. Table II shows that this minor design change makes marginal difference.

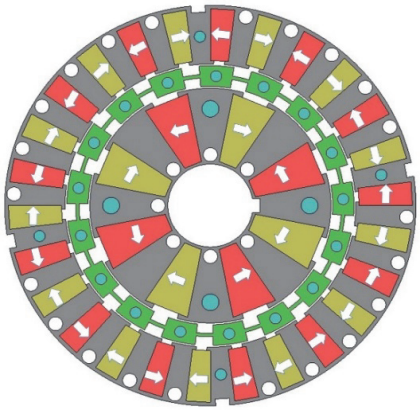

Fig. 5. The final laminated design (Design XIV) with magnet orientation shown.

TABLE II
TORQUE PERFORMANCE COMPARISON

Design	Torque [Nm]	Torque density [Nm/L]	Torque ripple [Nm]		Bridge Type*
			Outer rotor	Inner rotor	
Original	115	156.6	0.2	0.4	n
I	119.6	161.9	0.42	1.5	n
II	111	150.2	-	-	n
III	119	161.0	-	-	n
IV	113	152.9	-	-	n
V	111.8	151.3	-	-	n
VI	112.8	152.7	0.2	0.1	n
VII	105.2	142.1	2.2	0.4	i
VIII	103.5	140.0	0.75	0.25	m
IX	96.9	131.0	0.2	0.14	o
X	105.2	142.4	2.2	0.6	i
XI	95.8	129.7	0.175	0.14	o
XII	105.8	143.2	0.9	0.4	i
XIII	103	139.4	0.3	0.15	m
XVI	103.1	139.5	0.35	0.2	m

*Key: n = no bridge
o = outer radius bridge
i = inner radius bridge
m = middle bridge

III. FIELD AND TORQUE ANALYSIS

The radial and azimuthal magnetic flux density field values within the Design XIV magnetic gearbox are shown in Fig. 6 the saturation around the inner and outer rotor bridges is clearly apparent. The finite element analysis (FEA) calculated torque and torque ripple for Design XIV is plotted in Fig. 7 - Fig. 9 for the peak torque condition. A very low torque ripple was calculated.

IV. EXPERIMENTAL PROTOTYPE

The experimental prototype drawing for the MG is shown in Fig. 10. The outer and inner rotors are held in place using both a keyway and end-plates. The central cage rotor (rotor 2) is held together using end-plates and magnetic steel rods. The rods are made of magnetic steel and run through the center of the cage rotor bars. The MG on the test-stand is shown in Fig 11. The rotor laminations and inner rotor (without mag-

nets) are shown in Fig. 12. The measured torque and torque ripple at peak torque condition is shown in Fig. 13 and Fig. 14. Unfortunately, the torque was significantly lower than expected. The peak torque was measured to be only T_2 = 70.2Nm (95Nm/L) which is 25% lower than calculated. The torque ripple is also significantly higher than calculated. The reason for the lower peak torque and higher torque ripple is discussed in the next section.

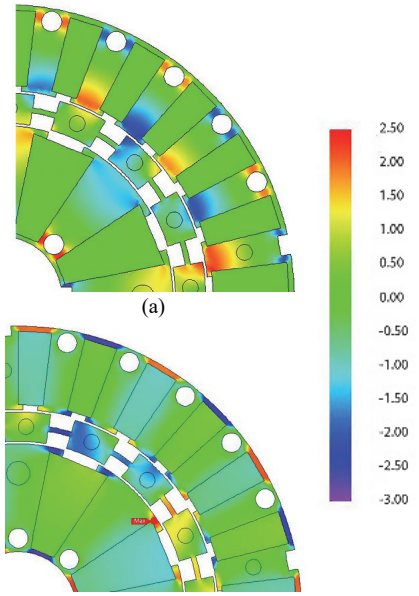

Fig. 6.(a) Radial flux density, B_r, and (b) azimuthal flux density, B_θ surface plot for Design XIV.

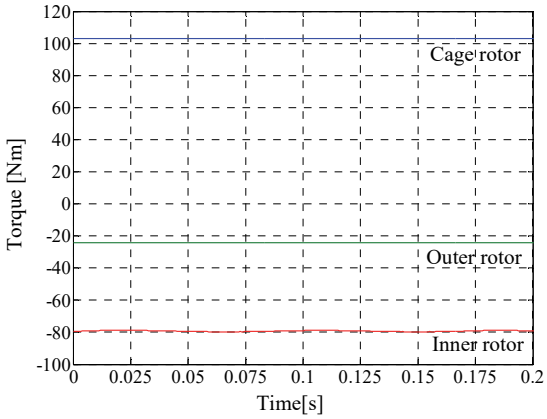

Fig. 7. Calculated torque as a function of time at peak torque condition

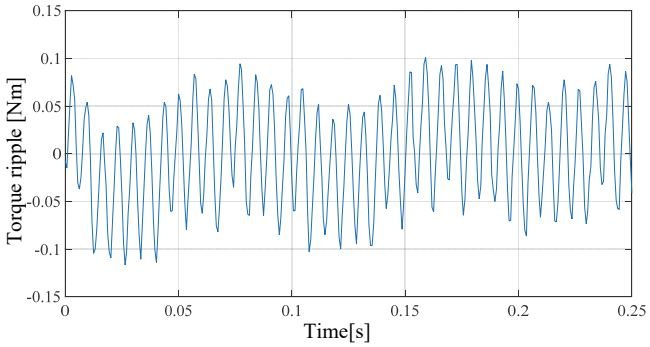

Fig. 8. High-speed (inner rotor) torque ripple

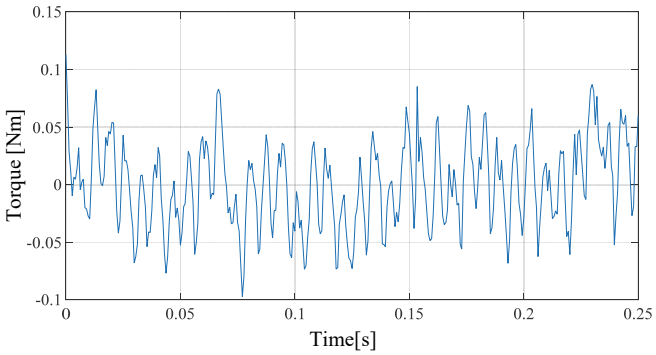

Fig. 9. Low-speed rotor torque ripple

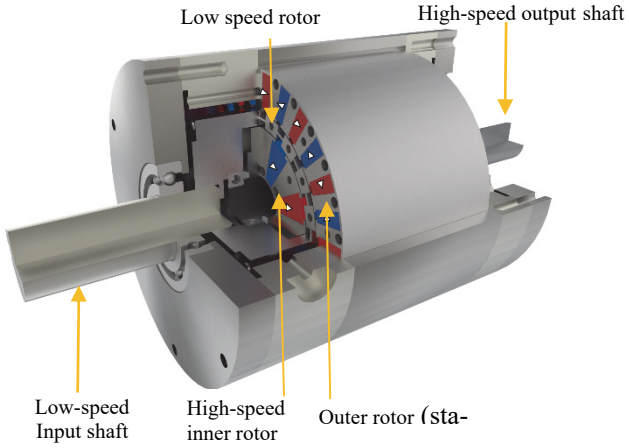

Fig. 10 Mechanical assembly drawing

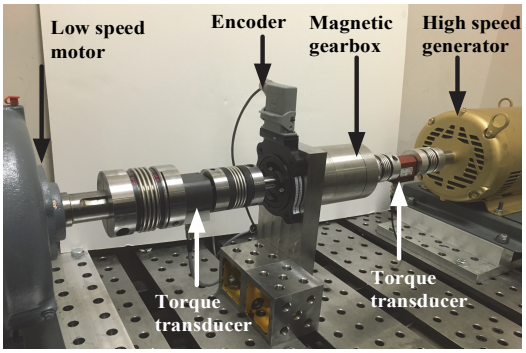

Fig. 11 Mechanical testing setup

V. Discrepancy Analysis

In order to understand why the MG had significantly lower torque than expected the MG was disassembled (multiple times) and the magnetic flux density of the inner rotor when surrounded by air was measured. The field measurements are shown in Fig. 15 while Fig 16 compares the expected 4th order fundamental field value with the measured. It can be noted that the measured value is significantly lower than what was expected. Fig. 15 shows that the magnet's residual flux density had to be lowered to B_r = 0.84 T in order to obtain a match. By measuring the individual magnets, as shown in Fig. 17 on can clearly see that the magnet field is far lower than expected. The authors believe that the magnets were demagnetized during earlier testing. The initial laminated MG design, not shown here, had an inferior endplate retaining

structure that resulted in the end plates not properly centering the rotors. This resulted in an eccentricity and it is believed that significant heating occurred that demagnetized the magnets. The authors then modified the design (to that shown in Fig. 10) to ensure that the design was more robust. Although the problem that created the demagnetization is believe to be fixed the degraded magnetization remains. The authors know of no papers discussing the thermal analysis of a MG and this is clearly an area that requires further investigation.

When the inner and outer magnet residual flux density, B_r, values were reduced to match the average value measured in Fig. 17 the calculated peak torque using FEA was determined to be $T_2 = 70.6$ Nm which very close to the measured value.

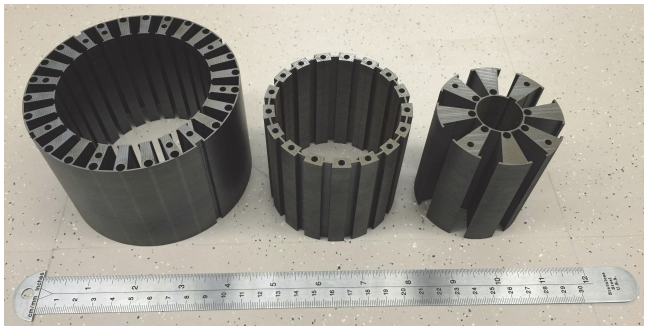

(a)

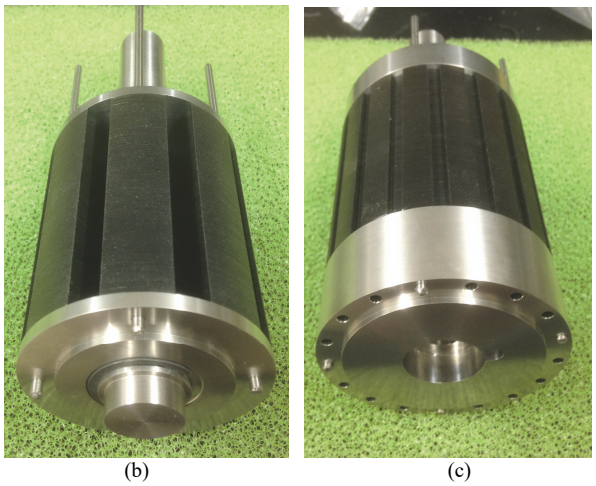

(b) (c)

Fig. 12 (a) Rotor laminations (b) inner rotor (c) cage rotor (rotor 2)

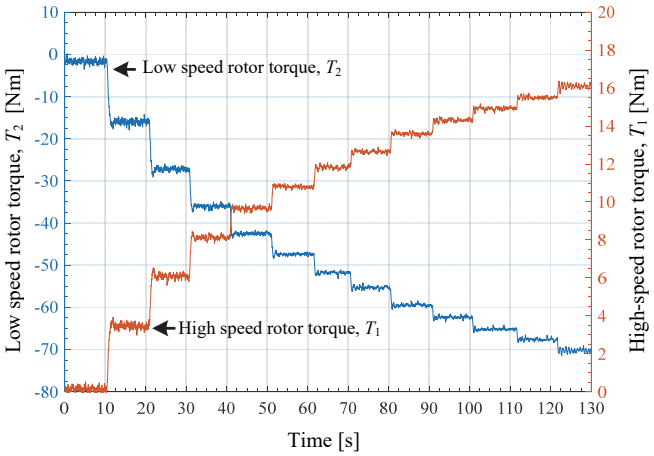

Fig. 13. Measured torque vs. time on low speed (rotor 2) and high-speed rotor (rotor 1).

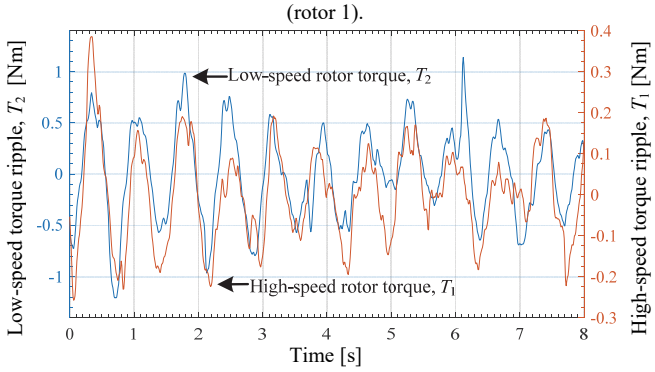

Fig. 14. Measured torque ripple vs. time on low speed (rotor 2) and high-speed rotor (rotor 1) at peak torque condition

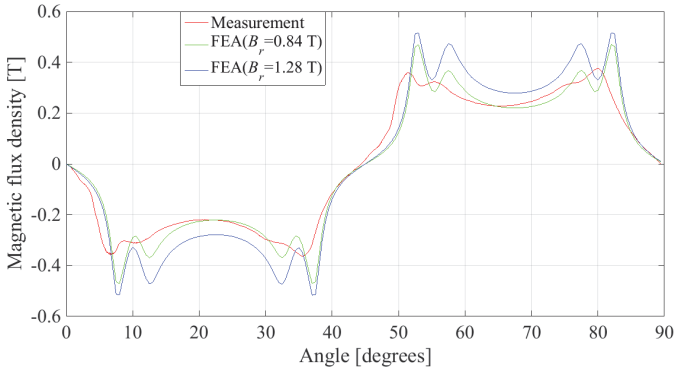

Fig. 15. Inner rotor field comparison when inner rotor is surrounded by air for (a) measured inner rotor field, (b) finite element calculated field for $B_r = 0.84$T and (c) for $B_r = 1.28$T.

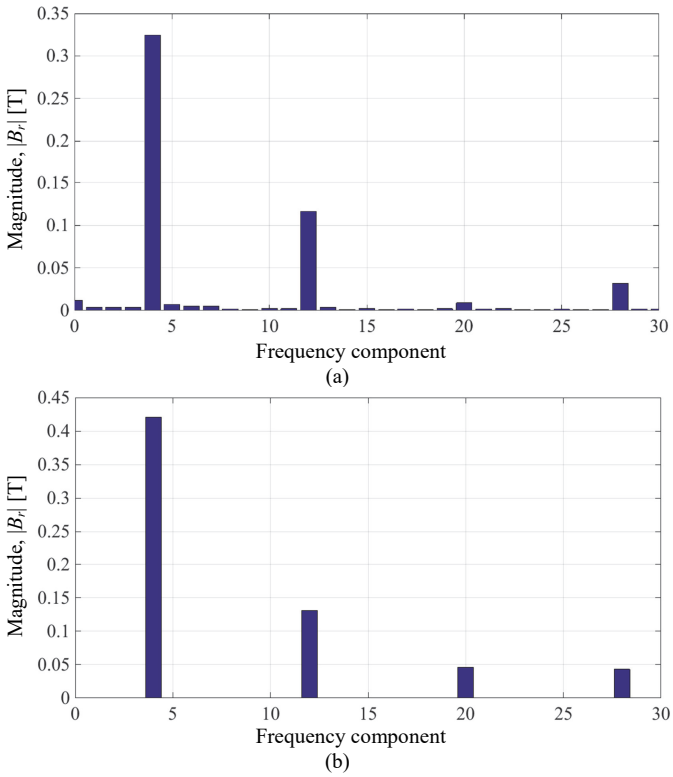

Fig. 16. Spatial harmonic analysis of inner rotor field for (a) measured and (b) calculated radial magnetic flux density.

The MG had to be disassembled multiple times in order to determine the cause of the lower than expected torque. The repeated disassembly and reassembly of the MG resulted in the introduction of geometric asymmetries in the rotor parts, it is believed that this caused the higher torque ripple than was predicted using FEA. Earlier testing indicated a lower torque ripple however only the final assembled MG torque ripple is reported here.

If the mechanical structure is designed as expected there are two primary magnetic material factors that will affect the peak torque of the MG. They are the magnet and steel residual magnetic flux density, B_r. A sensitivity analysis was conducted to asertain how these two magnetic properties affected the torque. The results are shown in Fig. 18. The percentage change in the torque when the magnets' B_r changes clearly dominates and is relatively linear.

Conclusion

A new laminated flux focusing MG mechanical structure was presented that is relatively easy to assemble and the cage rotor does not need to rely on epoxy or other complex fabrication steps to construct it. The experimentally measured peak torque density was measured to be 70.2Nm (95Nm/L) this is 25% lower than was predicted. It was determined that the torque was lower than expected due to the magnets being de-magnetized.

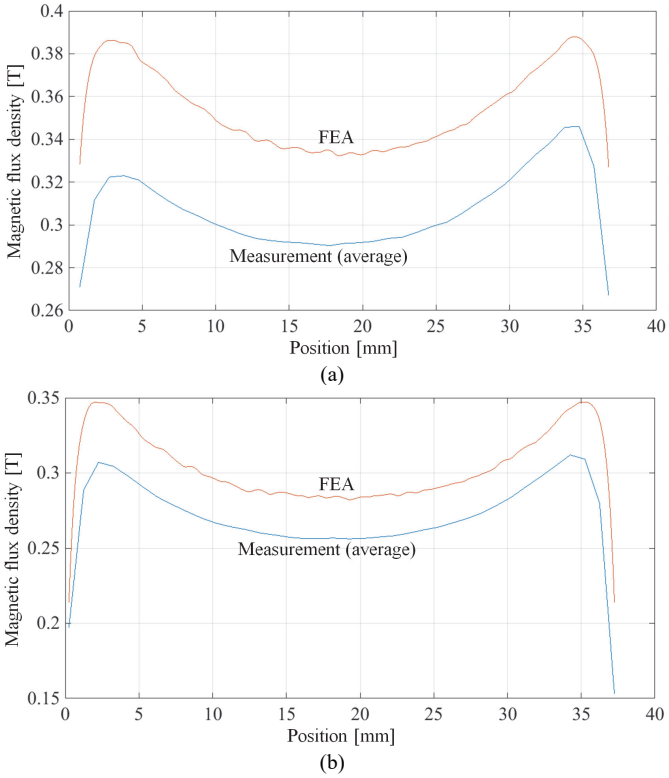

Fig. 17.(a) Inner magnets field comparison and (b) outer magnet field comparison along the central axial length of the magnet.

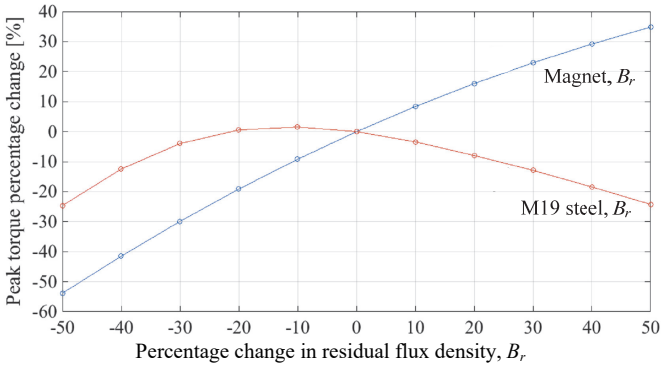

Fig. 18. The relationship between the percentage change in peak torque with the percentage change in the B_r of the M19 steel and NdFeB magnet material

Aknowlegements

The authors would gratefully like to thank the JMAG corporations for the use of their FEA software. This material is based upon work partially supported by the Department of Energy under Grant No. DE-EE0006801 as well as a North Carolina Coastal Studies Ocean Energy Grant.

References

[1] T. B. Martin, "Magnetic Transmission," USA Patent 3,378,710, 1968.

[2] K. Atallah, S. D. Calverley, and D. Howe, "Design, analysis and realisation of a high-performance magnetic gear," *IEE Proc.-Electr. Power Appl.,* vol. 151, pp. 135-143, 2004.

[3] K. K. Uppalapati, W. Bomela, J. Bird, M. Calvin, and J. Wright, "Experimental Evaluation of Low Speed Flux Focusing Magnetic Gearboxes," *IEEE Trans. on Ind. Appl.,* vol. 50, pp. pp. 3637 – 3643, Nov/Dec 2014.

[4] K. K. Uppalapati, J. Z. Bird, J. Wright, J. Pitchard, M. Calvin, and W. Williams, "A magnetic gearbox with an active region torque density of 239Nm/L," in *IEEE 2014 Energy Conv. Cong. Expo.*, pp. 1422-1428. 2014.

[5] K. K. Uppalapati and J. Z. Bird, "An iterative magnetomechanical deflection model for a magnetic gear," *IEEE Trans. Mag.,* vol. 50, Article #7005904, 2014.

[6] P. O. Rasmussen, T. O. Andersen, F. T. Jorgensen, and O. Nielsen, "Development of a high-performance magnetic gear," *IEEE Trans. Ind. Appl.,* vol. 41, pp. 764-770, 2005.

[7] P. O. Rasmussen, T. V. Frandsen, K. K. Jensen, and K. Jessen, "Experimental Evaluation of a Motor-Integrated Permanent-Magnet Gear," *IEEE Trans. Ind. Appl.,* vol. 49, pp. 850-859, 2013.

[8] S. Gerber and R. J. Wang, "Design and Evaluation of a Magnetically Geared PM Machine," *IEEE Trans. Magn.,* vol. 51, pp. 1-10, 2015.

[9] T. V. Frandsen, P. O. Rasmussen, and K. K. Jensen, "Improved motor intergrated permanent magnet gear for traction applications," in *IEEE 2012 Energy Conv. Cong. Expo.*, Raleigh, NC, pp. 3332 - 3339, Sept. 2012.

[10] N. W. Frank and H. A. Toliyat, "Analysis of the concentric planetary magnetic gear with strengthened stator and interior permanent magnet inner rotor," *IEEE Trans. Ind. Appl.,* vol. 47, pp. 1652-1660, July 2011.

[11] E. Gouda, "Transmission Planetaire Magnetique Etude, Optimisation et Realisation " Ph.D. Disertation, Nancy Université, France, 2011.

[12] L. Jian, K. T. Chau, and J. Z. Jiang, "A magnetic-geared outer-rotor permanent-magnet brushless machine for wind power generation," *IEEE Trans. on Ind. Appl.,* vol. 45, pp. 954-962, 2009.